Article

Characterization of Conformational Exchange of a Histidine Side Chain: Protonation, Rotamerization, and Tautomerization of His61 in Plastocyanin from *Anabaena variabilis*

Mathias A. S. Hass, D. Flemming Hansen, Hans E. M. Christensen, Jens J. Led, and Lewis E. Kay

J. Am. Chem. Soc., **2008**, 130 (26), 8460-8470 • DOI: 10.1021/ja801330h • Publication Date (Web): 07 June 2008

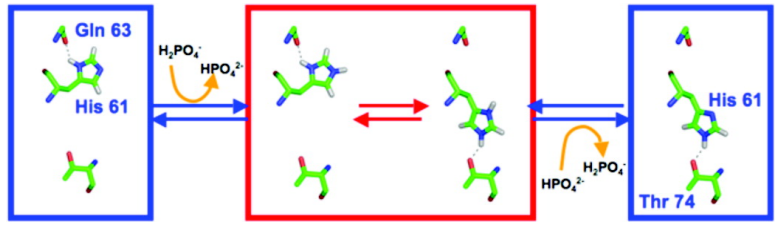

More About This Article

Additional resources and features associated with this article are available within the HTML version:

- Supporting Information
- Links to the 2 articles that cite this article, as of the time of this article download
- Access to high resolution figures
- Links to articles and content related to this article
- Copyright permission to reproduce figures and/or text from this article

View the Full Text HTML

J|A|C|S
ARTICLES

Published on Web 06/07/2008

Characterization of Conformational Exchange of a Histidine Side Chain: Protonation, Rotamerization, and Tautomerization of His61 in Plastocyanin from *Anabaena variabilis*

Mathias A. S. Hass,[†] D. Flemming Hansen,[‡] Hans E. M. Christensen,[§] Jens J. Led,[†] and Lewis E. Kay*[,‡]

Department of Chemistry, University of Copenhagen, Universitetsparken 5, DK-2100 Copenhagen Ø, Denmark, Departments of Molecular Genetics, Biochemistry, and Chemistry, University of Toronto, Toronto, Ontario, Canada M5S 1A8, and Department of Chemistry, The Technical University of Denmark, 2800 Lyngby, Denmark

Received February 26, 2008; E-mail: kay@pound.med.utoronto.ca

Abstract: A model describing conformational exchange of His 61 in plastocyanin from *Anabaena variabilis* is presented. A detailed picture of the exchange dynamics has been obtained using solution NMR relaxation measurements, chemical shift titrations, and structural information provided by a high-resolution crystal structure of the protein. A three-site model for chemical exchange that involves interconversion among the tautomeric and protonated forms of the histidine side chain with rates that are fast on the NMR chemical shift time scale can account for all of the data. In general, in the limit of fast exchange, it is not possible to obtain separate measures of chemical shift differences and populations of the participating states using NMR. However, we show here that when the data mentioned above are combined, it is possible to extract values of all of the parameters that characterize the exchange process, including rates, populations, and chemical shift changes, and to provide cross-validations that establish their accuracy. The methodology is generally applicable to the study of histidine side chain dynamics, which can play an important functional role in many protein systems.

Introduction

Histidine residues are found in the active sites of numerous proteins, where they are involved in catalysis,[1] pH regulation,[1] metal binding,[2] and phosphorylation.[3,4] A key feature of this amino acid is its imidazole side chain, which can exist in a variety of different protonation states, including a pair of neutral tautomer forms and a fully protonated, charged conformer.[5] Because histidines often have pK_a values that are close to physiological pH,[6] the imidazole group is likely to exist in a dynamic equilibrium among these various states. Exchange between these different forms constitutes a mechanism by which the activity of a protein can be modulated or proton transfer between an enzyme and a substrate can be mediated.[1,7,8] The chemical properties of histidines can be further modulated by side-chain rotamerizations involving the $C^{\alpha}-C^{\beta}$ and/or the $C^{\beta}-C^{\gamma}$ bond. It is noteworthy that a combination of ring flips (i.e., 180° χ_2 rotations) and tautomerizations can interconvert a nitrogen with a lone pair, a protonated nitrogen, and a C−H group at any of the δ and ε positions of the imidazole ring, largely without changing the space occupied by the side chain. In a confined, asymmetric protein environment, these different rotamers have different chemical properties. The multitude of conformations and potentially different chemical properties accessible through protonation and rotamerization enables histidine residues to act as switches in proteins in a variety of different contexts.[9] Therefore, it is of great interest to investigate the dynamic aspects of interchange among histidine conformations.

As early as 1965, it was recognized that NMR spectroscopy is a powerful probe of histidine residues located in active sites of proteins.[10] It is now well-established that NMR studies can identify the protonation state(s) of the imidazole ring and distinguish between different tautomers,[11–14] information that is difficult to obtain from X-ray crystallography, where hydrogen

[†] University of Copenhagen.
[‡] University of Toronto.
[§] The Technical University of Denmark.

(1) Fersht, A. *Structure and Mechanism in Protein Science: A Guide to Enzyme Catalysis and Protein Folding*; W. H. Freeman and Company: New York, 1998.
(2) Jensen, M. R.; Hass, M. A. S.; Hansen, D. F.; Led, J. J. *Cell. Mol. Life Sci.* **2007**, *64*, 1085–1104.
(3) Puttick, J.; Baker, E. N.; Delbaere, L. T. J. *Biochim. Biophys. Acta* **2008**, *1784*, 100–105.
(4) Dutta, R.; Qin, L.; Inouye, M. *Mol. Microbiol.* **1999**, *34*, 633–640.
(5) Reynolds, W. F.; Peat, I. R.; Freedman, M. H.; Lyerla, J. R. *J. Am. Chem. Soc.* **1973**, *95*, 328–331.
(6) Wüthrich, K. *NMR of Proteins and Nucleic Acids*; John Wiley & Sons: New York, 1986.
(7) Barnard, E. A. *Annu. Rev. Biochem.* **1969**, *38*, 677–732.
(8) Raines, R. T. *Chem. Rev.* **1998**, *98*, 1045–1065.
(9) Day, S. M.; Westfall, M. V.; Fomicheva, E. V.; Hoyer, K.; Yasuda, S.; La Cross, N. C.; D'Alecy, L. G.; Ingwall, J. S.; Metzger, J. M. *Nat. Med.* **2006**, *12*, 181–189.
(10) Mandel, M. *J. Biol. Chem.* **1965**, *240*, 1586–1592.
(11) Day, R. M.; Thalhauser, C. J.; Sudmeier, J. L.; Vincent, M. P.; Torchilin, E. V.; Sanford, D. G.; Bachovchin, C. W.; Bachovchin, W. W. *Protein Sci.* **2003**, *12*, 794–810.
(12) Pelton, J. G.; Torchia, D. A.; Meadow, N. D.; Roseman, S. *Protein Sci.* **1993**, *2*, 543–558.
(13) Perez-Canadillas, J. M.; Garcia-Mayoral, M. F.; Laurents, D. V.; del Pozo, A. M.; Gavilanes, J. G.; Rico, M.; Bruix, M. *FEBS Lett.* **2003**, *534*, 197–201.

 10.1021/ja801330h CCC: $40.75

atoms are rarely observed. In addition, NMR spectroscopy is an established tool for studying conformational exchange processes on the microsecond-to-millisecond time scale.[15,16] The dynamics of histidine protonation and tautomerization reactions can be studied by NMR line shape analysis,[17] relaxation dispersion methods,[18] and related approaches[19] that involve manipulations of experimental conditions such as pH. However, such studies become complicated when the histidine can exist in more than two different conformations. In such cases, complete determination of the thermodynamic and kinetic parameters from NMR relaxation data is still a challenge.

In the present work, we have studied conformational exchange events surrounding protonation and tautomerization of His 61 in plastocyanin[20] from *Anabaena variabilis* (hereafter termed *A.v.* PCu) using solution NMR spectroscopy in combination with structural information obtained from a recent crystal structure of the protein.[21] His 61 is located on the surface of the molecule and, in contrast to the other histidine residues in the protein, does not coordinate copper. Previously, we have shown that protonation and deprotonation of His 61 in *A.v.* PCu give rise to enhanced transverse relaxation rates for the amide ^{15}N of residues in the vicinity of His 61,[19] with protonation kinetics that are inconsistent with a two-site process, in contrast to the case for His 92 of the same protein. Interestingly, the X-ray structure of *A.v.* PCu (PDB entry 2GIM) shows that the side chain of His 61 can exist in two different orientations[21] that may be related to the more complex exchange kinetics observed for this residue. The fact that the conformational exchange process of His 61 can be "sensed" by NMR spectroscopy and that there may be a structural rationale provided by X-ray crystallography makes this an attractive model system for studies of histidine side chain dynamics.

The aim of this study was to obtain a complete characterization of the His 61 conformational exchange process. Such a description is complicated by both the multisite nature of the exchange and the fact that it is fast on the NMR chemical shift time scale. Presumably, multisite exchange processes are very common in complex biological molecules, and a few reports on studies of such exchanging systems have emerged recently.[22–27] However, analysis of these processes can be difficult, especially in view of the fact that often only the peaks originating from the most populated of the exchanging conformers are directly observed in NMR spectra.[15] Therefore, the majority of NMR exchange studies that involve spin relaxation data do not go beyond the simple case of two-site interconversion. If the exchange is fast on the NMR chemical shift time scale, additional complications arise. In such cases, all of the resonances of a given nucleus in the different exchanging conformations merge into a single average signal. Although the exchange process affects the observed relaxation rate, it becomes difficult to extract values of all of the exchange parameters from the NMR relaxation data alone. Typically, this situation occurs when all of the interconversions are faster than 1500−2000 s^{-1}. Rates of histidine protonation−deprotonation reported in the literature are on the order of several to many thousands per second,[17,19,28,29] while the time scale for rotamerization depends on the protein environment, with the lifetimes of unhindered rotation in the picosecond-to-nanosecond range.[30–33] Thus, exchange between different histidine side chain conformations in general is likely to be in the fast regime.

When all of the interconversions are in the fast-exchange regime on the NMR time scale, it is impossible to quantify the differences in both chemical shifts and populations of various states exclusively from spin relaxation data, even in the simple two-site case. Therefore, additional information about one of these parameters must be obtained. In the case of exchange between protonated and deprotonated histidines, such information can be obtained from chemical shift titrations,[19] since the nitrogen chemical shifts of the tautomeric and protonated imidazole side chain moieties are known with good accuracy.[11–14] We show here that it is possible to derive a three-site exchange model for His 61 that involves χ_1 rotamerization, tautomerization, and protonation and to extract values of all of the parameters that define the motion of this system by combining a series of different kinds of experimental data. This series includes relaxation rates obtained from a variety of spin relaxation measurements involving the imidazole nitrogens of His 61 and the amide nitrogens of proximal residues that are sensitive to its ionization state, chemical shift titration data, known ^{15}N chemical shifts for the imidazole side chain, and structural information available from X-ray studies of the protein.[21]

Results and Discussion

His 61 Conformational Exchange Process. In a previous pH titration study of *A.v.* PCu,[19] we showed that ^{15}N chemical shifts of residues proximal to His 61 titrate with pK_a values between 6.9 and 7.3 at 25 °C, in agreement with the pK_a of this histidine and suggesting that these proximal residues are excellent probes of the His 61 ionization state. Furthermore, the titration profiles were well-described by equations derived assuming a process in the fast-exchange regime on the NMR chemical shift time scale.[19] Contributions to ^{15}N transverse relaxation rates (R_{ex}) that derive from dynamics on the microsecond-to-millisecond

(14) Shimahara, H.; Yoshida, T.; Shibata, Y.; Shimizu, M.; Kyogoku, Y.; Sakiyama, F.; Nakazawa, T.; Tate, S.; Ohki, S.; Kato, T.; Moriyama, H.; Kishida, K.; Tano, Y.; Ohkubo, T.; Kobayashi, Y. *J. Biol. Chem.* **2007**, *282*, 9646–9656.
(15) Palmer, A. G.; Kroenke, C. D.; Loria, J. P. In *Nuclear Magnetic Resonance of Biological Macromolecules*; Academic Press: San Diego, CA, 2001; Vol. 339, pp 204−238.
(16) Palmer, A. G. *Chem. Rev.* **2004**, *104*, 3623–3640.
(17) Sudmeier, J. L.; Evelhoch, J. L.; Jonsson, N. B. H. *J. Magn. Reson.* **1980**, *40*, 377–390.
(18) Kovrigin, E. L.; Loria, J. P. *Biochemistry* **2006**, *45*, 2636–2647.
(19) Hass, M. A. S.; Thuesen, M. H.; Christensen, H. E. M.; Led, J. J. *J. Am. Chem. Soc.* **2004**, *126*, 753–765.
(20) Hope, A. B. *Biochim. Biophys. Acta* **2000**, *1456*, 5–26.
(21) Schmidt, L.; Christensen, H. E. M.; Harris, P. *Acta Crystallogr.* **2006**, *D62*, 1022–1029.
(22) Malmendal, A.; Evenas, J.; Forsen, S.; Akke, M. *J. Mol. Biol.* **1999**, *293*, 883–899.
(23) Eisenmesser, E. Z.; Bosco, D. A.; Akke, M.; Kern, D. *Science* **2002**, *295*, 1520–1523.
(24) Grey, M. J.; Wang, C. Y.; Palmer, A. G. *J. Am. Chem. Soc.* **2003**, *125*, 14324–14335.
(25) Korzhnev, D. M.; Salvatella, X.; Vendruscolo, M.; Di Nardo, A. A.; Davidson, A. R.; Dobson, C. M.; Kay, L. E. *Nature* **2004**, *430*, 586–590.
(26) Sugase, K.; Dyson, H. J.; Wright, P. E. *Nature* **2007**, *447*, 1021–1025.
(27) Tolkatchev, D.; Xu, P.; Ni, F. *J. Am. Chem. Soc.* **2003**, *125*, 12432–12442.
(28) Hass, M. A. S.; Christensen, H. E. M.; Zhang, J.; Led, J. J. *Biochemistry* **2007**, *46*, 14619–14628.
(29) Lommen, A.; Canters, G. W. *J. Biol. Chem.* **1990**, *265*, 2768–2774.
(30) Millet, O.; Mittermaier, A.; Baker, D.; Kay, L. E. *J. Mol. Biol.* **2003**, *329*, 551–563.
(31) Gelin, B. R.; Karplus, M. *Proc. Natl. Acad. Sci. U.S.A.* **1975**, *72*, 2002–2006.
(32) Henzler-Wildman, K.; Kern, D. *Nature* **2007**, *450*, 964–972.
(33) Best, R. B.; Clarke, J.; Karplus, M. *J. Mol. Biol.* **2005**, *349*, 185–203.

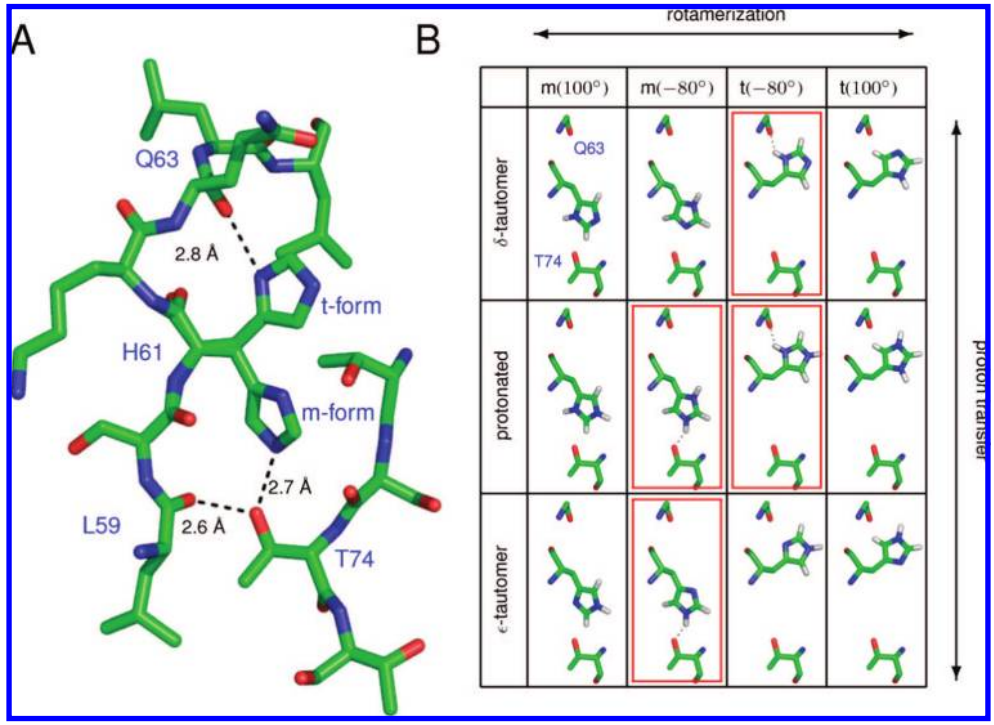

Figure 1. (A) The two distinct orientations of the imidazole side chain of His 61 in the crystal structure of *A.v.* PCu. (B) The 12 possible structures of His 61 that are consistent with the X-ray structure. The four structures framed in red are the ones that are stabilized by hydrogen bonding to either Gln 63 or Thr 74, as described in the text. The conformations are distinguished by the protonation state of the His 61 side chain (δ-tautomer, ε-tautomer, or protonated state), the χ_1 torsion angle [trans (t) or gauche-minus (m) form], and the χ_2 dihedral angle (100° or −80°).

time scale were also quantified, and while several residues had maximal R_{ex} values at pH = pK_a of His 61, the majority did not show this behavior. Interestingly, for the majority of the amide nitrogens, the expected quadratic dependence of R_{ex} on $\Delta\delta$, the chemical shift difference for His 61 in the protonated and neutral states, was not observed either.[19] These results suggest that the exchange process involving ionization of His 61 is more complex than a two-state process. In contrast, residues proximal to His 92 of the same protein showed large chemical shifts as a function of pH and titrated with a pK_a of 5.1, corresponding to the pK_a of His 92. Moreover, all of the amide nitrogens for these residues showed similar R_{ex} profiles as a function of pH, and there was a strong correlation between R_{ex} and $(\Delta\delta)^2$ for these amides. Thus, the exchange process involving ionization of His 92 is well-approximated by a two-state exchange event. This strongly suggests that the complexities noted for His 61 reflect an exchange process that is more complex than two-state and not artifacts associated with the NMR relaxation data or the analysis of the data.

Model of Conformational Exchange for His 61. Insight into the origin of the exchange behavior of His 61 can be derived from a recent 1.6 Å X-ray structure of *A.v.* PCu,[21] in which two conformations for this residue are observed (Figure 1A). The two conformers correspond to different χ_1 rotamers of the His 61 side chain that are related via a rotation of 108° around the $C^{\alpha}-C^{\beta}$ bond and are denoted here as the t and m forms (referring to the trans and gauche-minus conformations, respectively).[34] The protein was crystallized from a solution at pH 7.5, which is close to the pK_a of His 61,[19] so the exact protonation state of this histidine in the crystal structure remains uncertain. Because hydrogen atoms are not observed and it is not possible to distinguish between the electron densities of the nitrogen and carbon atoms in the imidazole ring, X-ray data in general do not uniquely define the conformation of a histidine side chain. Thus, for each of the two observed χ_1 rotamers of His 61, there are a pair of χ_2 rotamers [designated by the labels "(100°)" and "(−80°)", which indicate the approximate values of the χ_2 dihedral angle]. Furthermore, each of these four rotamers can exist in two different tautomeric forms or be fully protonated, so there is a total of 12 possible conformations of the His 61 side chain (Figure 1B). It is unlikely, however, that all 12 of these hypothetical conformers are significantly populated, and we assume that conformations that are stabilized by strong intramolecular hydrogen bonding are the ones that predominate in solution.

Figure 1 shows that there are two residues, Gln 63 and Thr 74, that potentially can form strong hydrogen bonds to the imidazole ring of His 61. The backbone carbonyl of Gln 63 can accept a hydrogen bond from the imidazole $N^{\delta 1}$ position when His 61 is in either the δ-tautomer or protonated state of the t(−80°) rotamer conformation. In addition to these two "structures", there are two others that are involved in hydrogen-bonding interactions with the side chain of Thr 74. The hydroxy group of Thr 74 can act as a hydrogen-bond donor and/or acceptor, and according to the crystal structure, it can donate a hydrogen bond to the backbone carbonyl of Leu 59, and/or accept a hydrogen bond from His 61. Both of these interactions are present simultaneously when the histidine side chain exists in either the ε-tautomer or protonated state of the m(−80°) rotamer conformation. In total, there are four stabilized conformations of His 61, which are highlighted in Figure 1 and denoted as ε-m(−80°), m(−80°)H^+, t(−80°)H^+, and δ-t(−80°); these are the structures included in our model.

(34) Lovell, S. C.; Word, J. M.; Richardson, J. S.; Richardson, D. C. *Proteins: Struct., Funct., Genet.* **2000**, *40*, 389–408.

Although the X-ray structure can be used to provide insight into the set of conformations that may be of relevance to the exchange process observed in solution, additional information is needed for construction of a scheme. This information can at least in part be obtained by qualitative solution NMR studies that probe changes in the line widths of (i) His 61 resonances or (ii) amide peaks derived from residues proximal to His 61 as a function of perturbations such as changes in pH or phosphate buffer concentration. At low pH values, where only the protonated forms of His 61 are significantly populated, the exchange broadening of proximal amide ^{15}N reporter probes is quenched.[19] This suggests that exchange between different conformers of protonated histidine [e.g., m(−80°)H$^+$ and t(−80°)H$^+$, which differ only in χ_1 angle and, as argued above, are likely candidates in a model of exchange] is very fast on the NMR chemical shift time scale. Molecular dynamics simulations[33,35] and NMR spin relaxation experiments[30,36] suggest that χ_1 angle rotations can occur on the picosecond-to-nanosecond time scale, and in the particular case of His 61, the X-ray structure shows that there are no steric clashes that could hinder the rotational path and thereby decrease the rotamerization rate.[21] However, rotamerization does involve breaking and forming of an intramolecular hydrogen bond, which also very likely occurs on the picosecond-to-nanosecond time scale,[1] as well as presumably minor rearrangements of solvent molecules. It is thus very likely that the overall rate of rotamerization, including the substitution of hydrogen bonds illustrated in Figure 1, occurs within the picosecond-to-nanosecond regime and therefore does not contribute to exchange broadening of the NMR signals. Thus, in the analysis of the NMR relaxation data (see below), different protonated forms of His 61 were treated as a single state, which in what follows is called CH$^+$. In contrast to the elimination of exchange contributions associated with acidic pH values, a corresponding quenching of the line broadening was not observed at alkaline pH (pH 9.5). At this pH, only neutral states of His 61 are significantly populated (see below). This suggests that interconversion between different neutral forms contributes to exchange broadening.

It is well-known that buffers, particularly phosphate ones, catalyze proton-transfer reactions.[17,29,37–39] Addition of increasing amounts of phosphate at neutral pH to a solution of *A.v.* PCu leads to the disappearance of line broadening (i.e., exchange becomes fast on the NMR chemical shift time scale), indicating that all of the rate-limiting steps involve proton transfer.[28] On the basis of the pH and phosphate results, we favor a scheme in which two neutral forms of His 61, A and B, exchange via a protonated form, CH$^+$:

$$A + H^+ \rightleftarrows CH^+ \rightleftarrows B + H^+ \quad (1)$$

In this model, the addition of phosphate that catalyzes proton transfer would be expected to quench exchange contributions, as observed, while at low pH values, where the protonated states of histidine are the predominant conformers, the effects of exchange would also be eliminated. In addition, at high pH values and low buffer concentrations, exchange between neutral forms of His 61 would occur through sparsely populated levels of CH$^+$, leading to line broadening of signals from residues proximal to the histidine. Alternative models that directly link A and B (i.e., without proton transfer) are disfavored because they are not consistent with quenching of exchange contributions by addition of high concentrations of phosphate. In this case, interconversion between A and B would not depend on phosphate concentration and would contribute to line broadening even at high phosphate concentrations.

The combination of the exchange model derived from the NMR relaxation data (eq 1) and the structural model inferred from the X-ray structure (Figure 1) suggest that the deprotonated forms A and B correspond to the ε-m(−80°) and δ-t(−80°) conformations, whereas CH$^+$ includes the conformations m(−80°)H$^+$ and t(−80°)H$^+$ undergoing fast exchange (see above). Therefore, in what follows, we consider the scheme

$$\varepsilon\text{-m}(-80°) + H_2PO_4^- \underset{k_{-1}}{\overset{k_1}{\rightleftharpoons}} CH^+ + HPO_4^{2-} \underset{k_2}{\overset{k_{-2}}{\rightleftharpoons}} \delta\text{-t}(-80°) + H_2PO_4^- \quad (2)$$

as the *simplest* model of exchange of His 61 that is consistent with the available X-ray and NMR data. We have included phosphate explicitly in eq 2 because (i) our studies below will be based on protein solutions in phosphate buffer; (ii) phosphates, like many other buffers, play an important role in biological proton-transfer reactions;[37] and (iii) spin relaxation studies with variable concentrations of phosphate provide a powerful means to extract the exchange parameters, as detailed below. Our goal in what follows is to evaluate the populations of ε-m(−80°), δ-t(−80°), and CH$^+$ in this model as well as the rate constants k_1, k_{-1}, k_2, and k_{-2}, in order to provide further support for the proposed exchange model and to show that all of the exchange data can be explained in terms of eq 2.

Calculation of Populations from Chemical Shift Titration Data. On the basis of the crystal structure of *A.v.* PCu,[21] results from a previous NMR relaxation study,[19] and the observed changes in amide line widths as a function of pH or phosphate buffer concentration, we have proposed a model of exchange for His 61 involving tautomerization/protonation of the imidazole ring, as outlined above. The equilibria involved in this model (eq 2) can be directly detected through observation of the ^{15}N NMR signals of the imidazole nitrogens[11–14] in ^{1}H−^{15}N multiple-bond correlated heteronuclear single-quantum coherence (HSQC) spectra that the link the protons H$^{\delta 2}$ and H$^{\varepsilon 1}$ with nitrogens via two-bond (H$^{\delta 2}$−N$^{\varepsilon 2}$, H$^{\varepsilon 1}$−N$^{\varepsilon 2}$, and H$^{\varepsilon 1}$−N$^{\delta 1}$) and three-bond (H$^{\delta 2}$−N$^{\delta 1}$) scalar couplings. However, the three-bond coupling is significantly smaller than the two-bond couplings in the deprotonated forms of the imidazole ring, giving rise to H$^{\delta 2}$−N$^{\delta 1}$ correlations that are weaker than the other cross-peaks.[12] Figure 2A shows the multiple-bond correlated ^{1}H−^{15}N map of His 61 at 5 °C in a buffer containing 80 mM phosphate in D_2O (pD* 7.6). In contrast, in the absence of buffer at neutral pH, cross-peaks from His 61 are not observed (Figure 2B), although signals from the other two histidines in *A.v.* PCu (His 39 and His 92) are present. For phosphate buffer concentrations on the order of a few millimoles per liter, the signals from His 61 are broadened beyond detection because the rate of exchange between protonation states approaches the large chemical shift difference between the protonated and deprotonated imidazole nitrogens (82 ppm[12]). Thus, unlike most exchange-broadened backbone amide ^{15}N signals, which enter the fast-exchange regime at exchange rates less than 2000 s^{-1} in spectra recorded at a static magnetic field strength of 500

(35) Gelin, B. R.; Karplus, M. *J. Am. Chem. Soc.* **1975**, *97*, 6996–7006.
(36) Xue, Y.; Pavlova, M. S.; Ryabov, Y. E.; Reif, B.; Skrynnikov, N. R. *J. Am. Chem. Soc.* **2007**, *129*, 6827–6838.
(37) Eigen, M. *Angew. Chem., Int. Ed. Engl.* **1964**, *3*, 1–19.
(38) Khalifah, R. G. *Proc. Natl. Acad. Sci. U.S.A.* **1973**, *70*, 1986–1989.
(39) Lindskog, S.; Coleman, J. E. *Proc. Natl. Acad. Sci. U.S.A.* **1973**, *70*, 2505–2508.

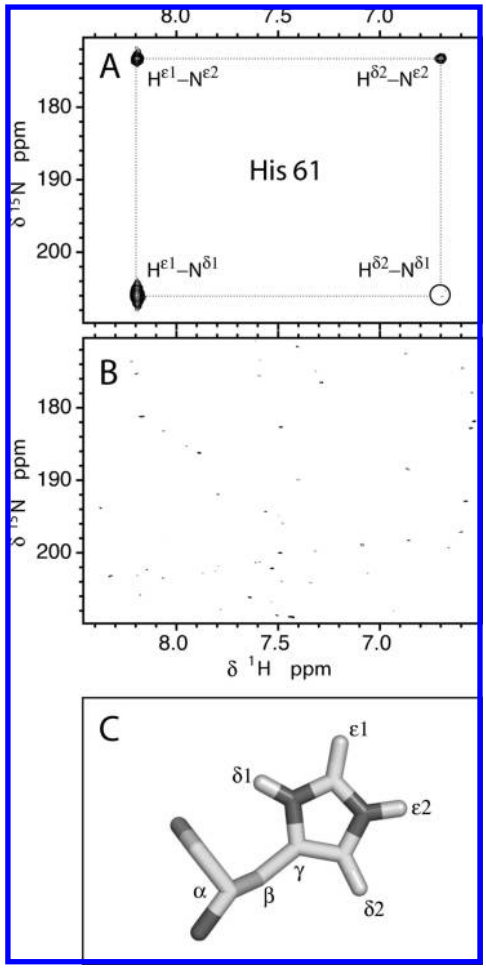

Figure 2. (A) Section from the 500 MHz $^1H-^{15}N$ multiple-bond correlated HSQC spectrum of *A.v.* PCu at 5 °C in 80 mM phosphate buffer, D_2O (pD* 7.6) uncorrected for the isotope effect, illustrating the correlation pattern observed for His 61. Assignments of each of the cross-peaks to specific correlations are indicated. (B) In the absence of phosphate, when exchange between conformers is no longer fast on the NMR chemical shift time scale, correlations are not observed for His 61 because of severe line broadening (although correlations for the other two histidine residues in the protein, His 39 and 92, are observed). (C) Structure of histidine showing the atom-numbering scheme.

MHz (^1H frequency), the imidazole nitrogens remain in the slow- or intermediate-exchange regime for values of the exchange rate constant (k_{ex}) less than the value of 25 000 s^{-1} that occurs at low phosphate concentrations. In 80 mM phosphate buffer, however, the exchange is sufficiently rapid that all four of the expected peaks are observed, with a pattern (assigned as indicated in Figure 2A) that is consistent with the presence of a large population of the ε tautomer. It should be noted that the $^{15}N^{\delta1}$ chemical shift is 210 ppm rather than 250 ppm as would be expected if only the ε tautomer were populated in solution (Table 1). This chemical shift deviation clearly indicates that the protonated form is also present at the applied pH. On the basis of the pattern of cross-peaks, the chemical shifts of the individual correlations, and the tabulated shifts of protonated and deprotonated imidazole nitrogens (see Table 1), approximately equal populations of the protonated and ε-tautomer species are predicted at pD* 7.6.

A quantitative analysis of the populations can be obtained from a pH titration of histidine ^{15}N chemical shifts. Over the complete range of pH values examined, only a single set of correlations was observed for His 61; this indicates a fast

Table 1. ^{15}N Chemical Shifts (ppm) for the Imidazole Side Chain of His 61

		$\delta_{N^{\varepsilon2}}$	$\delta_{N^{\delta1}}$
	δ-tautomer[a]	249.5	167.5
	ε-tautomer[a]	167.5	249.5
	protonated[a]	176.5	176.5
high-pH limit[d]	observed[b]	174.7	241.5
	calculated[c]	174.9	242.1
low-pH limit[e]	observed[b]	171.8	178.8
	calculated[c]	176.5	176.5

[a] Literature values[12] of ^{15}N chemical shifts for the histidine imidazole ring. [b] Obtained from a fit of the imidazole ^{15}N chemical shift titration data to eq 4. [c] His 61 ^{15}N chemical shifts back-calculated using eq 3 along with literature chemical shifts and populations from fits of chemical shift titration data. [d] Neutral His 61; the chemical shift is equal to δ_0 in eq 4. [e] Fully protonated His 61; the chemical shift is equal to $\delta_0 + \Delta\delta_{prot}$ in eq 4.

exchange process, in which the observed ^{15}N chemical shifts (δ_{obs}) can be expressed as

$$\delta_{obs} = p_{CH^+}\delta_{CH^+} + p_\varepsilon\delta_\varepsilon + p_\delta\delta_\delta \tag{3}$$

where p_{CH^+}, p_ε, and p_δ are the populations of the protonated, ε-tautomer, and δ-tautomer forms of His61, respectively, and δ_{CH^+}, δ_ε, and δ_δ are the corresponding chemical shifts, which are well-approximated by the literature values given in Table 1. Equation 3 can be recast as

$$\delta_{obs} = \frac{\Delta\delta_{prot}}{1 + 10^{[pH - pK_a]}} + \delta_0 \tag{4}$$

where

$$\delta_0 = \frac{\delta_\varepsilon}{1 + K_{\varepsilon\delta}} + \frac{\delta_\delta}{1 + K_{\varepsilon\delta}^{-1}} \tag{5}$$

$$\Delta\delta_{prot} = \delta_{CH^+} - \delta_0 \tag{6}$$

$$K_a = \frac{(p_\varepsilon + p_\delta)[H^+]}{p_{CH^+}} \tag{7}$$

$$K_{\varepsilon\delta} = \frac{p_\delta}{p_\varepsilon} \tag{8}$$

From these equations, it follows that the populations p_ε, p_δ, and p_{CH+} are given by

$$p_\varepsilon = \left(\frac{1}{1 + K_{\varepsilon\delta}}\right)\left(1 + \frac{[H^+]}{K_a}\right)^{-1}$$
$$p_\delta = \left(\frac{1}{1 + K_{\varepsilon\delta}^{-1}}\right)\left(1 + \frac{[H^+]}{K_a}\right)^{-1} \tag{9}$$
$$p_{CH^+} = \left(1 + \frac{K_a}{[H^+]}\right)^{-1}$$

Figure 3A shows a superposition of $^1H-^{15}N$ multiple bond-correlation maps of His 61 as a function of pH in a series of titrations where the phosphate concentration was kept constant at 50 mM to ensure that exchange was in the fast regime. In the pH titration series, signals could be followed up to pH 8.3; above this pH, the $H_2PO_4^-$ concentration was too low to ensure fast protonation of the imidazole ring (see eq 2). The titration of the ^{15}N chemical shifts with pH is shown in Figure 3B along with best fits to the data obtained using eq 4. Since the pK_a value of His 61 is unique (i.e., it differs from any other pK_a value in the protein by more than one unit[19]), $\Delta\delta_{prot}$, δ_0, and

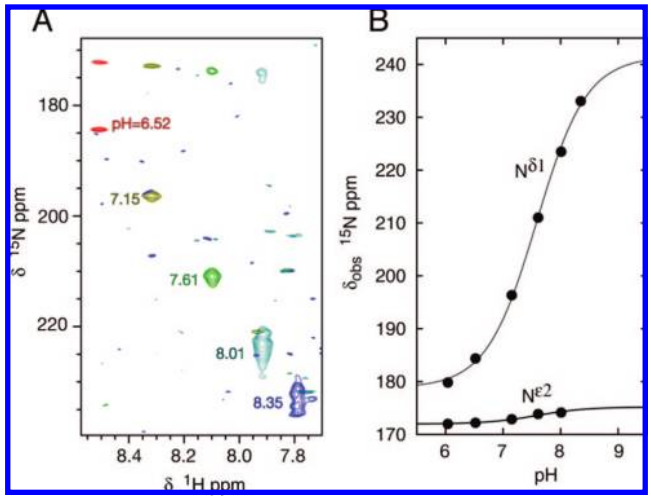

Figure 3. (A) Overlay of multiple-bond correlated $^{1}H-^{15}N$ spectra as a function of pH, showing the titration of the imidazole signals of His 61 of *A.v.* PCu at 5 °C in 50 mM phosphate buffer. (B) Fits of the ^{15}N chemical shifts to eq 4.

pK_a can be reliably determined from analysis of chemical shift titration curves.

The pK_a value obtained from imidazole titrations at 5 °C was 7.6 ± 0.1, which was further confirmed by fits of backbone amide titration curves (not shown). The $^{15}N^{\delta 1}$ and $^{15}N^{\varepsilon 2}$ δ_0 values obtained from the fitted titration curves in the high-pH limit (Figure 3B) were used to calculate the p_δ/p_ε ratio, since $p_\delta/p_\varepsilon = (\delta_\varepsilon - \delta_0)/(\delta_0 - \delta_\delta)$.[14] Values of 0.096 and 0.108 for p_δ/p_ε were obtained from the fits of the $^{15}N^{\delta 1}$ and $^{15}N^{\varepsilon 2}$ titration curves, respectively; the average value of the ratio was 0.102 ± 0.05. Thus, the populations of the δ and ε tautomers were 0.09 and 0.91, respectively, when His 61 was completely deprotonated. Using these results along with literature values of histidine imidazole nitrogen chemical shifts, we were able to calculate $^{15}N^{\delta 1}$ and $^{15}N^{\varepsilon 2}$ chemical shifts for His 61 in the high- and low-pH limits (Table 1) that were in excellent agreement with the measured values of δ_0 and $\Delta\delta_{prot} + \delta_0$, respectively.

Probing of the Exchange Properties of Spins Proximal to His 61. In order to probe the exchange process involving His 61 in more detail, we performed backbone amide ^{1}H and ^{15}N relaxation dispersion experiments at pH 9.5 in 0.5 mM phosphate buffer at 5 °C. At this high pH value, the imidazole of His 61 is predominantly in the neutral state; substitution of the values pK_a = 7.6 and $K_{\varepsilon\delta}$ = 0.10 (determined as described above) into eqs 9 yielded the values p_δ = 0.09, p_ε = 0.90, and p_{CH^+} = 0.01. Thus, $p_{CH+} < p_\delta < p_\varepsilon$, allowing the small population of CH^+ to be neglected and the exchange reaction to be approximated as a two-state process. Significant ^{15}N Carr−Purcell−Meiboom−Gill (CPMG) dispersion profiles were observed for seven nuclei (His 39, Ser 60, His 61, Gln 63, Leu 64, Ser 73, and Thr 74), while ^{1}H dispersion curves were obtained for Val 29, His 39, Asn 40, Val 41, Ser 60, His 61, Gln 63, Ser 73, Thr 74, Thr 75, and Glu 90. Some of the dispersion profiles are shown in Figure 4. The ^{15}N and ^{1}H dispersions (recorded at 500 MHz for ^{15}N and at 500 and 800 MHz for ^{1}H) were numerically fitted to a two-site model of chemical exchange that included data from all of the above-mentioned residues. The value of k_{ex} obtained from the global fit was 2200 ± 200 s^{-1} when the populations of the two exchanging states were set equal to those of the two tautomers

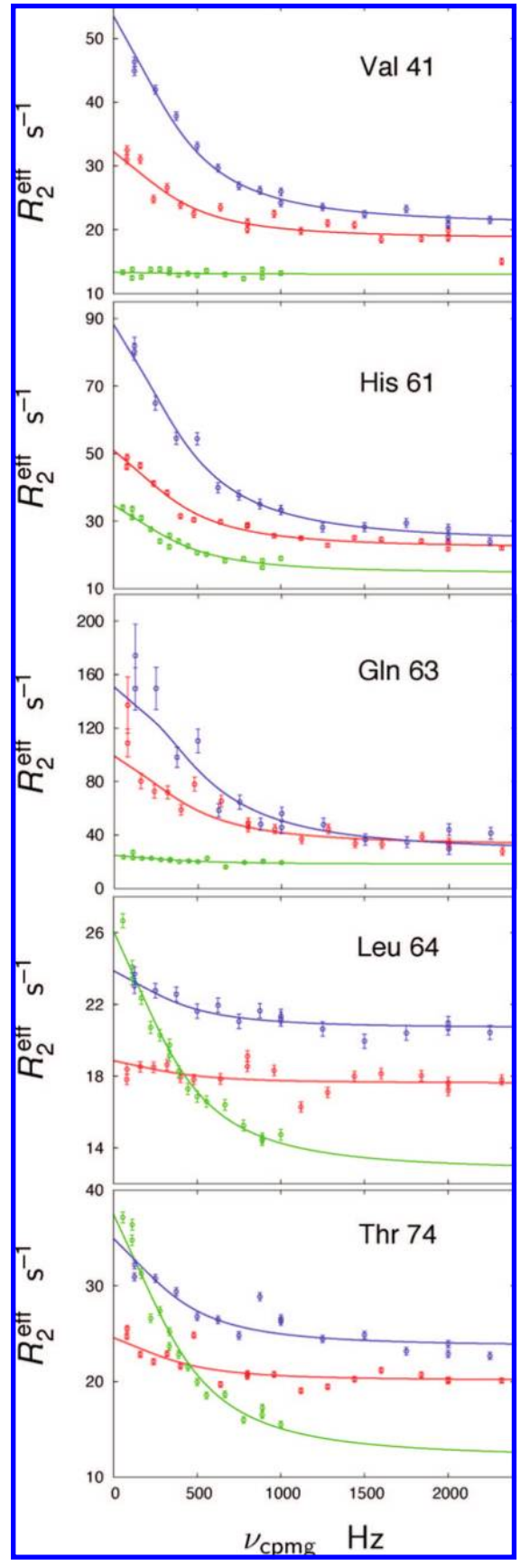

Figure 4. ^{15}N (500 MHz, green) and ^{1}H (500 MHz, red; 800 MHz, blue) CPMG relaxation dispersion curves for selected residues in *A.v.* PCu at pH 9.5 in 0.5 mM phosphate buffer at 5 °C. Solid lines were obtained from a global fit of the dispersion data to a two-site exchange model (see text).

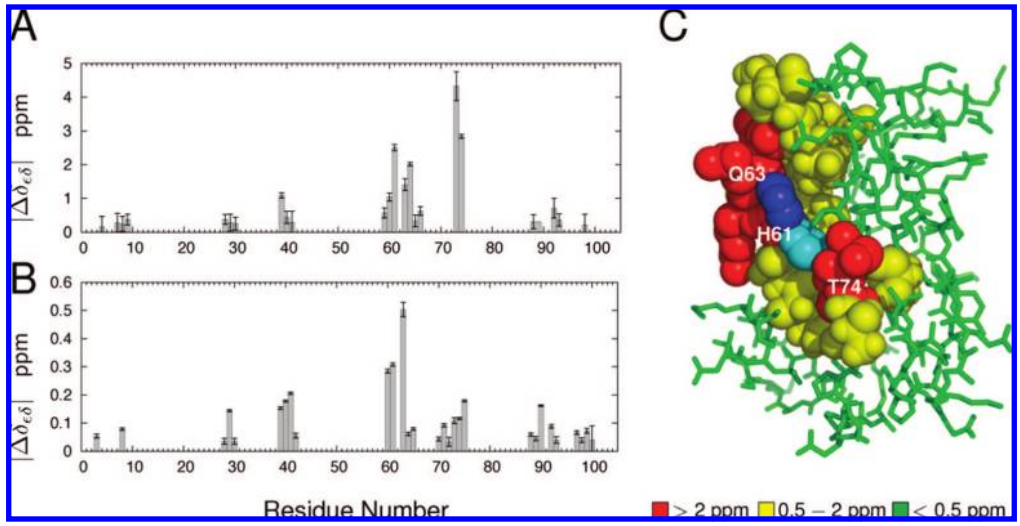

Figure 5. Absolute values of backbone amide (A) ^{15}N and (B) ^{1}H chemical shift differences resulting from exchange between the ε and δ tautomers of His 61, as determined from CPMG relaxation dispersion experiments at pH 9.5 in 0.5 mM phosphate buffer at 5 °C using values of p_δ and p_ε obtained from imidazole ^{15}N chemical shift titrations. (C) Structure of *A.v.* PCu color-coded according to values of $\Delta\delta = \{[\Delta\delta_{\varepsilon\delta}(^{15}\mathrm{N})]^2 + [5\Delta\delta_{\varepsilon\delta}(^{1}\mathrm{H})]^2\}^{1/2}$. The two χ_1 rotamers of the His 61 side chain are colored dark-blue (t form) and light-blue (m form).

of His 61. Values of k_{ex} from per-residue fits of dispersion data were all consistent and in good agreement with the rate obtained from the global analysis of the data, indicating that all of the dispersions were reporting on a single process. Despite the fact that only a small concentration of phosphate (0.5 mM) was used in the buffer in order to slow the exchange process as much as possible, it was nevertheless the case that exchange was fast on the NMR chemical shift time scale for a majority of the residues. Therefore, populations could not be extracted reliably from the dispersion data alone.

Panels A and B of Figure 5 show plots of the absolute values of the chemical shift differences $\Delta\delta_{\varepsilon\delta} = \delta_\delta - \delta_\varepsilon$ extracted from fits of amide ^{15}N and ^{1}H relaxation dispersion profiles, respectively; the $|\Delta\delta_{\varepsilon\delta}|$ values are color-coded onto the X-ray structure of the protein in Figure 5C. The largest differences are observed for Leu 59−Leu 65, Ser 71−Thr 75, and His 39−Val 42, with smaller shifts for several residues between Tyr 88 and Lys 100. Besides His 61, the largest shifts are noted for Gln 63, Thr 74, and neighboring residues. It was mentioned earlier that in the X-ray structure, Gln 63 and Thr 74 form hydrogen bonds with the t and m forms of His 61, respectively, and that according to the proposed model of exchange (eq 2), these residues would be expected to show large exchange contributions as a result of the interchange of the two orientations of the His 61 side chain (Figure 1). The results of the present analysis are thus consistent with and strengthen the proposed exchange model.

Although only absolute values $|\Delta\delta_{\varepsilon\delta}|$ (or $|\Delta\omega_{\varepsilon\delta}|$, for chemical shifts expressed in rad/s) can be obtained from fits of amide relaxation dispersion profiles, the signs of the ^{15}N shift differences can also be obtained.[40] This sign information is important for the analysis of R_2 relaxation rates that we will consider in the next section. In cases where exchange is close to intermediate, the chemical shift of the signal observed in the HSQC experiment will be shifted slightly from that in the heteronuclear multiple-quantum coherence (HMQC) data set, and the direction of this shift can be used to obtain the sign of $\Delta\delta_{\varepsilon\delta}$.[40] In addition, the peak positions depend on the static magnetic field strength, and thus, small but quantifiable differences in peak positions can be observed in HSQC data sets recorded at different fields; these differences can also can provide the missing sign information.[40]

HSQC and HMQC chemical shifts were obtained at pH 9.5 for the amide nitrogens proximal to His 61, where the exchange is well-approximated by a two-state process (see above). Under these conditions, the value of $\delta\nu_N$, the difference in the shifts extracted from HSQC and HMQC data sets, depends on the populations of the two tautomers, the exchange rate, $\Delta\delta_{\varepsilon\delta}$ for the ^{15}N nucleus, and $|\Delta\delta_{\varepsilon\delta}|$ for the one-bond-coupled ^{1}H nucleus, while the value of $\delta\sigma_N$, the difference in peak positions in HSQC spectra recorded at different static magnetic fields, depends on the populations of the two tautomers, the exchange rate, and $\Delta\delta_{\varepsilon\delta}$ for the ^{15}N nucleus.[40] The absolute values of these shifts, $|\delta\nu_N|$ and $|\delta\sigma_N|$, which can be calculated independently on the basis of the known exchange parameters, are compared with the corresponding observed values in Figure 6. Residues falling in the shaded (unshaded) areas are those for which $\Delta\delta_{\varepsilon\delta} = \delta_\delta - \delta_\varepsilon$ is positive (negative). The correlation coefficients for the plots were greater than 0.98, and the average ratios of observed and calculated values were 0.71 and 1.21 for $\delta\nu_N$ (Figure 6A) and $\delta\sigma_N$ (Figure 6B), respectively. The good agreement provides further support for the proposed exchange model for His 61.

Determination of Rates of Exchange between Tautomeric and Protonated Forms of His 61. The rates constants $k_{\pm1}$ and $k_{\pm2}$ for the interconversions between ε-m(−80°) and δ-t(−80°), respectively, and CH^+ (see eq 2) can be obtained from fits of the phosphate-concentration dependence of measured amide ^{15}N relaxation rates (R_2) for residues proximal to His 61. Values of R_2 were measured using a CPMG pulse train having a CPMG pulsing frequency (ν_{CPMG}) of 500 s^{-1} and subsequently fit to calculated values of $R_2(\nu_{CPMG} = 500\ \mathrm{Hz})$ obtained numerically on the basis of eq 2 following the procedure of Grey et al.[24] (see Data Analysis). For a system exchanging among three states according to eq 2, $R_2(\nu_{CPMG})$ is a function of $k_{\pm1}'$, $k_{\pm2}'$, $\Delta\omega_{\varepsilon\delta}$, $\Delta\omega_{prot}$ (see Data Analysis), and R_2^0, the intrinsic relaxation rate of the spin probe (assumed to be the same for all three states; see Data Analysis). The pseudo-first-order forward and reverse

(40) Skrynnikov, N. R.; Dahlquist, F. W.; Kay, L. E. *J. Am. Chem. Soc.* **2002**, *124*, 12352–12360.

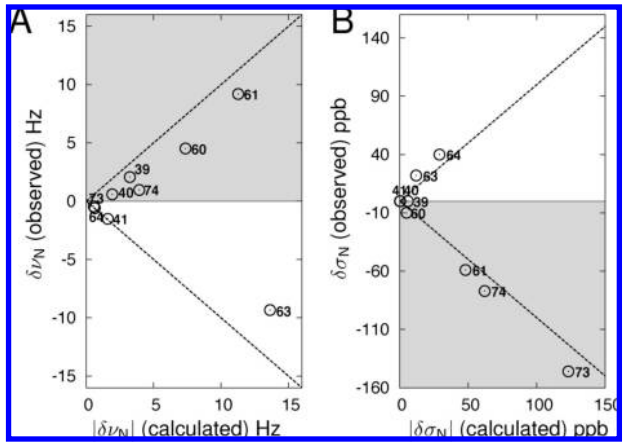

Figure 6. (A) Observed differences in ^{15}N shifts obtained from 500 MHz $^{1}H-^{15}N$ HSQC and HMQC spectra recorded at pH 9.5 in 0.5 mM phosphate buffer at 5 °C ($\delta\nu_N = \delta_{HSQC} - \delta_{HMQC}$) plotted vs absolute values of $\delta\nu_N$ calculated on the basis of exchange parameter values extracted from fits of CPMG relaxation dispersion profiles and pH titrations. (B) Observed differences in ^{15}N peak positions measured in HSQC spectra recorded at 800 and 500 MHz ($\delta\sigma_N = \delta_{800\ MHz} - \delta_{500\ MHz}$) plotted vs calculated values of $\delta\sigma_N$. Residues that fall in the shaded (unshaded) areas are those for which $\Delta\delta_{\varepsilon\delta} = \delta_\delta - \delta_\varepsilon$ is positive (negative).

rate constants k_j' and k_{-j}' ($j = 1, 2$) depend on the phosphate concentrations according to the relations $k_j' = k_j[H_2PO_4^-] + k_j^0$ and $k_{-j}' = k_{-j}[HPO_4^{2-}] + k_{-j}^0$, where k_j^0 and k_{-j}^0 are the rate constants in the absence of phosphate buffer. The number of fitting parameters can be reduced by imposing the condition of chemical equilibrium, so that the following relations apply: $k_{-1} = k_1K_a/[K_{phos}(1 + K_{\varepsilon\delta})]$ and $k_{-2} = k_2K_a/[K_{phos}(1 + K_{\varepsilon\delta}^{-1})]$, where K_{phos} is the acid-dissociation constant of $H_2PO_4^-$; and $k_{-1}^0 = k_1^0p_\varepsilon/p_{CH^+}$ and $k_{-2}^0 = k_2^0p_\delta/p_{CH^+}$, where the values of p_δ, p_ε, and p_{CH+} at a given pH can be calculated from eqs 9 since pK_a and $K_{\varepsilon\delta}$ are known. In this work, a value of 7.21 was used for K_{phos} (ionic strength 0.1 M, 25 °C).[41]

In addition to the chemical shift differences $\Delta\omega_{\varepsilon\delta}$ that were measured as described in the previous section, fits of $R_2(\nu_{CPMG})$ depend also on $\Delta\omega_{prot}$ (see Data Analysis). These can be obtained from pH titrations of amide chemical shifts, as described above (see eqs 3 and 4) and in more detail in the Supporting Information, where titration curves and fitted data are presented for several residues proximal to His 61. Values of $\Delta\delta_{\varepsilon\delta}$ and $\Delta\delta_{prot}$ are listed in Table 2.

The values of k_1, k_2, k_1^0, and k_2^0 presented in Table 3 were obtained from fits of the phosphate dependence of the ^{15}N R_2 values for Ser 60, His 61, Gln 63, Leu 64, and Thr 74, the five residues with the most pronounced phosphate-dependent amide ^{15}N transverse relaxation rates (Figure 7). The values of the rate constants k_1 and k_2 for proton transfer from $H_2PO_4^-$ to the δ and ε nitrogen positions of His 61, respectively, are similar, as expected in view of the fact that the nonprotonated nitrogens of the two χ_1 rotamers considered in the exchange model are approximately equally exposed to solvent.[21] However, the values differ from those measured for free imidazole (10^9 M^{-1} s^{-1} at 25 °C[44]), reflecting the protein environment surrounding His 61 and, to a lesser extent, the decreased temperature employed in the present study.

Verification of Extracted Parameter Values. The extracted values of the rate constants (Table 3) are based on analysis of relaxation data obtained from backbone amide groups that report on the His 61 exchange process. An independent view is provided by ^{15}N imidazole relaxation rates, which monitor the same three-site exchange process. Indeed, since all of the parameters of the exchanging system are known, it is possible to quantitatively predict the dependence of the His 61 ^{15}N imidazole line widths on the phosphate buffer concentration. Agreement with experimental results can serve as a validation of the measured exchange parameters. The line widths were calculated using an approach similar to the one employed to obtain $R_2(\nu_{CPMG} = 500\ Hz)$, as described above and in Data Analysis; in this case, R_2 in the free-precession limit ($\nu_{CPMG} = 0$) is desired. Figure 8A shows cross sections along F_1 (the ^{15}N dimension) of two-dimensional multiple-bond HSQC spectra (see Figure 2A) recorded at 500 MHz and 5 °C with pH = pK_a = 7.6 and different concentrations of phosphate buffer as listed. It is clear that the line widths depend critically on buffer concentration. Interestingly, the downfield resonance corresponding to $^{15}N^{\delta1}$ moved 4 ppm upfield during the course of the titration, although the pH was maintained within ±0.05 unit. This displacement was most likely caused by the increase in ionic strength during the course of the titration. It is expected that increasing the ionic strength would stabilize the charged form of the imidazole ring and thereby increase its pK_a, which in turn would lead to an upfield shift. However, significant movements of the $^{15}N^{\delta1}$ signal were observed only for phosphate buffer concentrations larger than 100 mM. Figure 8 compares the experimental R_2 values estimated from the measured line widths (circles) with those calculated using the exchange parameters (solid curves). The agreement is good, validating both the exchange model used and the parameter values obtained.

As an interesting aside, it is worth emphasizing that because the difference in chemical shifts of protonated and deprotonated imidazole ^{15}N atoms is on the order of 80 ppm, the line shape analysis described above can monitor exchange events that take place on a time scale of hundreds of nanoseconds, a time regime that is usually not accessible to other NMR methods. The rate constant values listed in Table

Table 2. Amide $\Delta\delta$ Values (ppm) for Residues Most Affected by the Three-Site Conformational Exchange of His 61 in *A.v.* PCu

	^{15}N		^{1}H	
residue	$\Delta\delta_{prot}$[a]	$\Delta\delta_{\varepsilon\delta}$	$\Delta\delta_{prot}$[b]	$\lvert\Delta\delta_{\varepsilon\delta}\rvert$
H39	−0.12	1.09	0.00	0.15
N40	−0.06	0.44	0.04	0.18
V41	−0.59	−0.23	−0.17	0.21
S60	0.50	1.05	0.12	0.28
H61	−2.32	2.50	0.06	0.31
K62	0.77	4−5[c,d]	0.25	−
Q63	0.27	−1.41	0.05	0.50
L64	0.91	−2.02	0.09	0.06
S73	0.93	4−7[d]	−0.07	0.11
T74	−0.48	−0.48	0.03	0.12

[a] From ref 19. [b] From ref 42. [c] The sign of $\Delta\delta_{\varepsilon\delta}$ could not be determined. [d] The value could not be reliably determined from fits of CPMG dispersion curves.

(41) *Handbook of Chemistry and Physics*, 74th ed.; CRC press: Boca Raton, FL, 1993.

(42) Hass, M. A. S.; Jensen, M. R.; Led, J. J. *Proteins: Struct., Funct., Bioinf.* **2008**, *72*, 333–343.

(43) Press, W. H.; Flannery, B. P.; Teukolsky, S. A.; Vetterling, W. T. *Numerical Recipies in C*; Cambridge University Press: Cambridge, U.K., 1988.

(44) Eigen, M.; Hammes, G. G. *Adv. Enzymol. Relat. Subj. Biochem.* **1963**, *25*, 1–38.

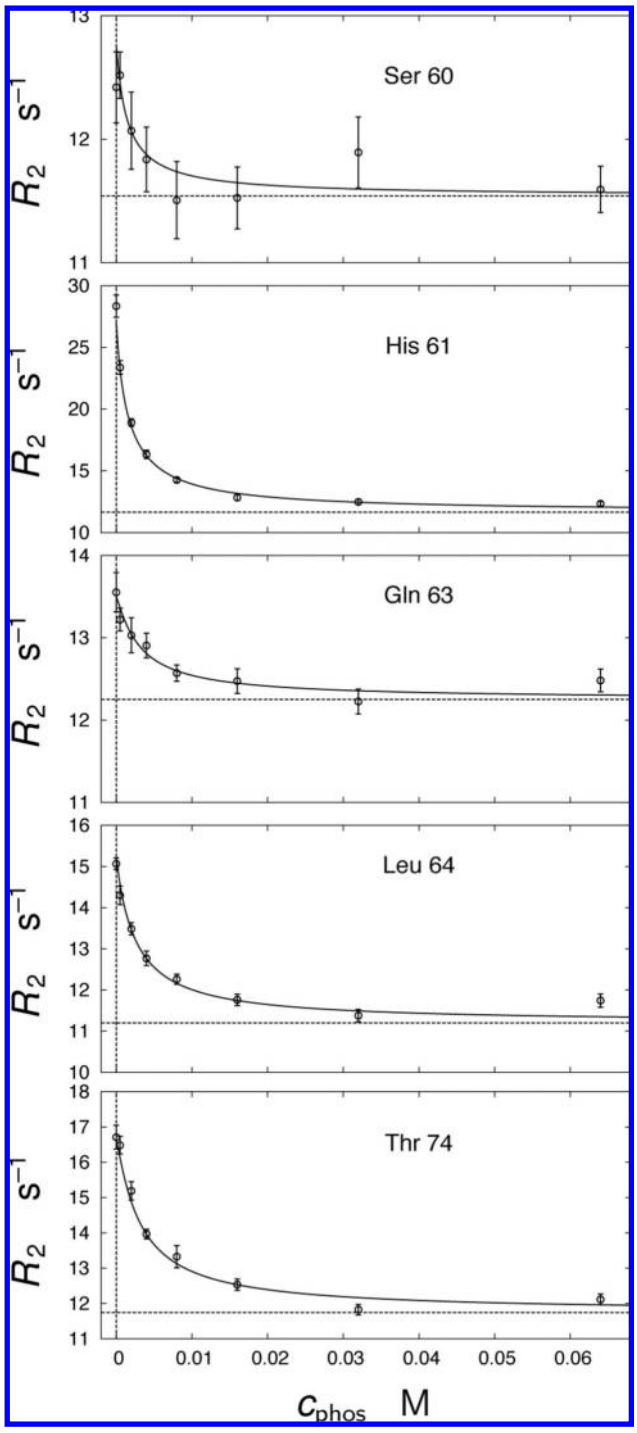

Figure 7. Backbone ^{15}N relaxation rates (R_2) as functions of phosphate buffer concentration (c_{phos}) for five residues in *A.v.* PCu that report on the His 61 conformational exchange process. The solid lines were obtained from a global fit of the experimental data to the three-site exchange model (eq 2). The dashed horizontal lines indicate the R_2^0 values obtained from the fit. Experiments were carried out at 5 °C, pH 7.65, and 500 MHz.

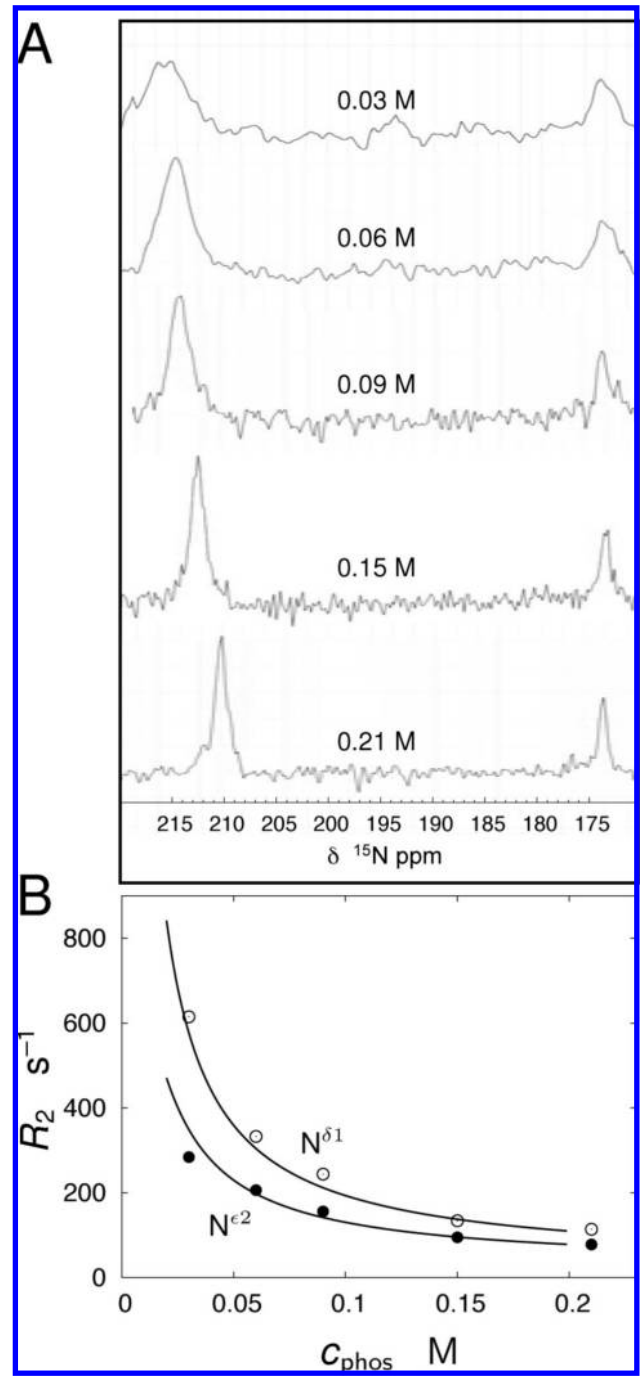

Figure 8. (A) F_1 (^{15}N) cross sections from 500 MHz $^1H-^{15}N$ multiple-bond correlation spectra (taken at an F_2 chemical shift corresponding to the His 61 $H^{\epsilon 1}$ resonance position) for five different phosphate buffer concentrations (given in the labels above the spectra). (B) Dependence of the imidazole ^{15}N R_2 values on the phosphate buffer concentration at pH 7.6, 5 °C, and 500 MHz. The experimental R_2 values (circles) were obtained from the line widths of the imidazole signals in (A). The solid curves are the rates as a function of the phosphate buffer concentration calculated from numerical simulations based on the three-site exchange model of eq 2 using the parameter values given in Tables 1 and 3.

3 indicate that the His 61 exchange process enters the microsecond time regime at a phosphate buffer concentration of 50 mM.

Concluding Remarks

Here we have presented a complete analysis of a three-site, fast-exchange system in which His 61 of *A.v.* PCu exchanges among states that involve side-chain protonation, tautomerization, and χ_1 rotamerization. The exchange process can be characterized by combining NMR measurements with structural insights provided by X-ray studies of the protein. Although the work focuses on a single histidine in only one protein, the methodology used may have implications for studies of many other systems. For example, His 64 in human carbonic anhydrase II plays a critical role in proton transport that is required for

Table 3. Rate Constant Values Obtained from the Phosphate-Buffer Dependence of ^{15}N Backbone Amide R_2 Values at 5 °C[a]

k_1 (10^7 M^{-1} s^{-1})	k_2 (10^7 M^{-1} s^{-1})	k_{-1} (10^6 M^{-1} s^{-1})[b]	k_{-2} (10^5 M^{-1} s^{-1})[b]	k_1^0 (10^3 s^{-1})	k_2^0 (10^3 s^{-1})	k^0_{-1} (10^3 s^{-1})[c]	k^0_{-2} (10^2 s^{-1})[c]
2.1 ± 0.4	1.0 ± 0.1	7.8 ± 1.5	3.8 ± 0.4	3.8 ± 0.5	4.6 ± 0.4	3.9 ± 0.5	4.8 ± 0.4

[a] Uncertainties were estimated using Monte Carlo simulations.[43] [b] Calculated from the value of the corresponding forward rate constant and the equilibrium constant values pK_a = 7.6, $K_{\varepsilon\delta}$ = 0.102 (determined from chemical shift titration data) and pK_{phos} = 7.21 (from ref 41) (see text). [c] Calculated from k_1^0 or k_2^0 using $k^0_{-1} = k_1^0 p_\varepsilon / p_{CH^+}$ or $k^0_{-2} = k_2^0 p_\delta / p_{CH^+}$, respectively, at pH 7.65 (see text).

catalytic turnover in this enzyme.[38,39] High-resolution crystal structures have recently shown that His 64 is present in two distinct χ_1 rotameric states, and a combination of X-ray, NMR, and computer-simulation results indicate that each of the rotamers corresponds to a different tautomer of the imidazole ring.[14,45–47] It has been suggested that tautomerization and χ_1 rotation of His 64 are part of the proton-transfer mechanism. It seems likely that methods similar to those used in this work to study His 61 of *A.v.* PCu could be applied to investigate the dynamics of His 64 of carbonyic anhydrase, leading to new insights into the mechanism of action of this enzyme. Histidine dynamics are also implicated in the function of members of the serine protease family.[18,48] A recent NMR study of the Asp 121−His 119 catalytic dyad in RNase A showed that His 119 exists in an equilibrium between two χ_1 rotameric states that may couple to other functionally important motions of the protein.[18] In addition, motions of His 57 in the catalytic triad of α-lytic protease were detected by NMR, and it has been postulated that such dynamics could involve ring flips.[48] The dynamics of histidine residues have been probed using NMR for the past several decades.[17,19,29,49] The present work shows that a combination of high-resolution structural information and state-of-the-art NMR dynamics measurements can be used to obtain a detailed quantitative picture of what these motions might be.

Materials and Methods

^{2}H- and ^{15}N-labeled *A. variabilis* PCu Samples. ^{2}H,^{15}N-labeled *A.v.* PCu was produced as described in detail in the Supporting Information. The level of deuteration of the samples used in this work was 60%, as estimated by comparing the NMR signal intensity of the amide region to that of the aliphatic region of the one-dimensional ^{1}H spectrum of ^{2}H,^{15}N-labeled and ^{15}N-labeled protein. The sample concentration used in the experiments was 1 mM, and the solvent was 100 mM NaCl in 90:10 (v/v) H_2O/D_2O with variable amounts of phosphate added and having variable pH depending on the application, as listed in the text.

NMR Spectroscopy. Each data set was recorded at 5 °C on a Varian Inova 500 or 800 MHz (^{1}H frequency) spectrometer equipped with a room-temperature probe. To observe imidazole ^{15}N signals, ^{1}H−^{15}N multiple-bond correlation data sets were measured at 500 MHz using a non-sensitivity-enhanced HSQC pulse sequence in which the INEPT (insensitive nuclei enhanced by polarization transfer) periods were set to 21.7 ms, an integer multiple of $1/^1J_{NH}$, where $^1J_{NH}$ is the one-bond ^{1}H−^{15}N scalar coupling constant.[12] The choice of this delay significantly attenuated undesired signals from backbone amides. Experiments to measure populations and chemical shift values were carried out at a series of different pH values in the 6−8 range using 50 mM phosphate buffer to ensure that exchange was in the fast regime. Acquisition times of 14 and 64 ms were recorded in t_1 and t_2, respectively, with 32−512 scans for each free-induction decay, depending on the pH. The ^{15}N carrier frequency was positioned at 205 ppm. Spectra were also recorded in order to measure ^{15}N line widths as a function of phosphate concentration over the range 0.03−0.21 M at 5 °C, pH 7.65, and 500 MHz; for these spectra, the acquisition time in t_1 was set to 40 ms and ^{15}N carrier frequency at 195 ppm.

Amide ^{1}H constant-time CPMG relaxation dispersion experiments[50] were performed at 500 and 800 MHz at pH 9.5 and 5 °C using a constant-time relaxation delay of 25 ms, during which a variable number of refocusing pulses were applied. A series of 19 or 16 experiments were performed with $\nu_{CPMG} = 1/(2\tau_{CP})$ ranging from 80 or 120 to 2000 Hz at 500 or 800 MHz, respectively, where τ_{CP} is the delay between successive 180° pulses in the CPMG sequence. Because the degree of deuteration was only 60%, a selective ^{1}H RE-BURP pulse[51] was applied in the middle of the constant-time CPMG relaxation interval in order to selectively refocus amide protons. ^{15}N constant-time,[52] relaxation-compensated[53] relaxation dispersion experiments were performed at 500 MHz using a constant-time relaxation delay of 36 ms. A series of 18 ν_{CPMG} values in the range 55−1000 Hz was used. The signs of ^{15}N chemical shift differences extracted from relaxation dispersion were obtained using the method of Skrynnikov et al.[40] by recording HMQC and HSQC data sets at both 500 and 800 MHz.

^{15}N R_2 experiments[14] as a function of phosphate concentration (pH 7.65, 5 °C, 500 MHz) were performed in order to determine the rate constants $k_{\pm1}$ and $k_{\pm2}$ in eq 2. Nine relaxation delays (ν_{CPMG} = 500 Hz) varying from 0 to 96 ms were obtained.

Data Analysis. All of the data sets were processed using the nmrPipe/nmrDraw suite of programs[54] and analyzed as described previously.[19,55] Analysis of the relaxation dispersion data was carried out using in-house software that is available upon request.

As mentioned in the Results and Discussion, values of the exchange rate constants (eq 2) were determined from numerical fits of backbone amide ^{15}N R_2 values as a function of phosphate concentration. Values of $R_2(\nu_{CPMG} = 500\ Hz)$ were computed using the approach of Grey et al.[24] In their formalism,

$$R_2^{calc}(\nu_{CPMG}) = R_2^0 - \nu_{CPMG} \ln \lambda \tag{10}$$

where λ is the largest eigenvalue of the matrix **L**:

$$\mathbf{L} = \exp\left(\frac{\mathbf{A}^\dagger}{2\nu_{CPMG}}\right)\exp\left(\frac{\mathbf{A}}{2\nu_{CPMG}}\right) \tag{11.1}$$

The matrix **A** in eq 11.1 is defined as $\mathbf{A} = \mathbf{K} + \mathbf{\Delta\Omega}$, where the matrices **K** and $\mathbf{\Delta\Omega}$ are given by

$$\mathbf{K} = \mathbf{S}^{-1}\begin{bmatrix} -k_1' & k_{-1}' & 0 \\ k_1' & -(k_{-1}' + k_{-2}') & k_2' \\ 0 & k_{-2}' & -k_2' \end{bmatrix}\mathbf{S},$$

$$\text{where} \quad \mathbf{S} = \begin{bmatrix} \sqrt{p_\varepsilon} & 0 & 0 \\ 0 & \sqrt{p_{CH^+}} & 0 \\ 0 & 0 & \sqrt{p_\delta} \end{bmatrix} \tag{11.2}$$

and

$$\mathbf{\Delta\Omega} = i\begin{bmatrix} 0 & 0 & 0 \\ 0 & \Delta\omega_{prot} + \dfrac{\Delta\omega_{\varepsilon\delta}}{1 + K_{\varepsilon\delta}^{-1}} & 0 \\ 0 & 0 & \Delta\omega_{\varepsilon\delta} \end{bmatrix} \tag{11.3}$$

(45) Fisher, S. Z.; Maupin, C. M.; Budayova-Spano, M.; Govindasamy, L.; Tu, C.; Agbandje-McKenna, M.; Silverman, D. N.; Voth, G. A.; McKenna, R. *Biochemistry* **2007**, *46*, 2930–2937.
(46) Fisher, Z.; Prada, J. A. H.; Tu, C.; Duda, D.; Yoshioka, C.; An, H. Q.; Govindasamy, L.; Silverman, D. N.; McKenna, R. *Biochemistry* **2005**, *44*, 1097–1105.
(47) Maupin, C. M.; Voth, G. A. *Biochemistry* **2007**, *46*, 2938–2947.
(48) Haddad, K. C.; Sudmeier, J. L.; Bachovchin, D. A.; Bachovchin, W. W. *Proc. Natl. Acad. Sci. U.S.A.* **2005**, *102*, 1006–1011.
(49) Meadows, D. H.; Markley, J. L.; Cohen, J. S.; Jardetzky, O. *Proc. Natl. Acad. Sci. U.S.A.* **1967**, *58*, 1307–1313.

where $\Delta\omega_{prot} = \omega_{CH^+} - [\omega_\varepsilon/(1 + K_{\varepsilon\delta}) + \omega_\delta/(1 + K_{\varepsilon\delta}^{-1})]$, $\Delta\omega_{\varepsilon\delta} = \omega_\delta - \omega_\varepsilon$, and other terms have been defined previously. Finally, the elements of $\mathbf{A}^\dagger$ are defined by $A_{ij}^\dagger = A_{ji}^*$, where * denotes complex conjugation. Here we have assumed that all three states relax with the same intrinsic relaxation rate, R_2^0. Values of R_2^{calc} were fitted to experimentally determined rates for a number of residues proximal to His 61 using software written in MATLAB (The MathWorks, Inc.), with the value of R_2^0 adjusted so that the exchange contribution to transverse relaxation (the second term in eq 10) approaches zero in the limit of infinitely high phosphate concentration.

In order to extract the exchange rates, the chemical shift differences $\Delta\delta_{\varepsilon\delta}$ and $\Delta\delta_{prot}$ for the backbone amide nitrogens are needed. As described above, $\Delta\delta_{\varepsilon\delta}$ values were obtained from relaxation dispersion measurements. In contrast, values of $\Delta\delta_{prot}$ were obtained from previous studies,[19] where the titration of ^{15}N backbone amide chemical shifts as a function of pH (Figure S1 in the Supporting Information) were fit to the relation

$$\delta_{obs} = \frac{\Delta\delta_{prot}}{1 + 10^{[pH - pK_a]}} + \frac{\Delta\delta_{other}}{1 + 10^{[pH - pK_{other}]}} + \delta_0 \qquad (12)$$

The first term in eq 12 accounts for the contribution to the chemical shift from the protonation of His 61, the second term includes all of the contributions from other titrations in the protein, and δ_0 is the amide chemical shift in the high-pH limit (i.e., when all of the titrations are complete). Since the pK_a value for His 61 differs by more than one unit from any other pK_a value in *A.v.* PCu, $\Delta\delta_{prot}$ can be reliably determined from the chemical shift titration curves.

Acknowledgment. We thank Ranjith Muhandiram (Toronto), Philipp Neudecker (Toronto), and Lise-Lotte Jespersen (Lyngby) for technical assistance. This study was supported by grants from the Canadian Institutes of Health Research (CIHR) and the Natural Sciences and Engineering Council of Canada and by Danish Natural Science Research Council Grant 21-04-0519, Carlsbergfondet Grant 1624/40, and Novo Nordisk Fonden Grant 2003-11-28. D.F.H. acknowledges postdoctoral fellowships from the CIHR and the Danish Agency for Science, Technology and Innovation (J. No. 272-05-0232).

Supporting Information Available: A detailed description of sample preparation procedures and Figure S1 showing pH titration curves of backbone amide ^{15}N chemical shifts for a set of residues proximal to His 61. This material is available free of charge via the Internet at http://pubs.acs.org.

JA801330H

(50) Ishima, R.; Torchia, D. A. *J. Biomol. NMR* **2003**, *25*, 243–248.
(51) Geen, H.; Freeman, R. *J. Magn. Reson.* **1991**, *93*, 93–141.
(52) Tollinger, M.; Skrynnikov, N. R.; Mulder, F. A. A.; Forman-Kay, J. D.; Kay, L. E. *J. Am. Chem. Soc.* **2001**, *123*, 11341–11352.
(53) Loria, J. P.; Rance, M.; Palmer, A. G. *J. Am. Chem. Soc.* **1999**, *121*, 2331–2332.
(54) Delaglio, F.; Grzesiek, S.; Vuister, G. W.; Zhu, G.; Pfeifer, J.; Bax, A. *J. Biomol. NMR* **1995**, *6*, 277–293.
(55) Mulder, F. A. A.; Skrynnikov, N. R.; Hon, B.; Dahlquist, F. W.; Kay, L. E. *J. Am. Chem. Soc.* **2001**, *123*, 967–975.